Journal of Membrane Science 323 (2008) 247–256

Contents lists available at ScienceDirect

Journal of Membrane Science

journal homepage: www.elsevier.com/locate/memsci

Predicting the effect of membrane spacers on mass transfer

Abhishek Shrivastava, Satish Kumar, E.L. Cussler*

Department of Chemical Engineering and Materials Science, University of Minnesota, Minneapolis, MN 55455, United States

ARTICLE INFO

Article history:
Received 7 November 2007
Received in revised form 16 May 2008
Accepted 23 May 2008
Available online 5 June 2008

Keywords:
Ultrafiltration
Reverse osmosis
Concentration polarization
Spacers

ABSTRACT

Like many separation processes, ultrafiltration and reverse osmosis are often compromised by concentration polarization. Such polarization can be mitigated by static mixers and other flow barriers placed as spacers next to the membrane surface. These spacers can be shaped like ladders, herringbones, and helices. The effect of these spacers can be successfully predicted without adjustable parameters from extensions of the Lévêque equation. The predictions are in agreement with results of computational fluid mechanics and with electrochemical experiments. They supply a tool for optimizing spacer design.

The shortage of potable water will be a major problem of the next 20 years, probably compromising the lives of 40% of the world's population. This shortage will have a social impact on the same scale as that of increased energy prices. One major route to decreasing this water shortage will be membrane separations, especially because these processes remove impurities less than a micron in size. Ultrafiltration can remove viruses from groundwater; reverse osmosis can remove salt from seawater.

Both ultrafiltration and reverse osmosis are often compromised by concentration polarization [1]. This polarization occurs when water passes quickly through the membrane and impurities accumulate on the feed (upstream) side of the membrane. In ultrafiltration, these impurities can foul the membrane; in reverse osmosis, the resulting concentrated solution at this surface compromises the water flux across the membrane. In either case, the membrane process has a lower productivity.

Because concentration polarization is a widely recognized problem, many have tried to reduce the effect with spacers or static mixers set close to the membrane's surface [2]. The spacers try to disrupt the flow near the membrane, causing better mixing in the feed solution. Many shapes have been tried. Spacers shaped like ladders were a frequent early choice, later replaced by spacers shaped like diamonds. Designs for static mixers, which normally aim at enhancing bulk mixing, should also work for this application [3]. In all these cases, the results are less than would be expected from studies of turbulent heat transfer. The reason is that flow in membrane separations is almost always laminar, the consequence of the small channels chosen to get large membrane areas per process volume. These large areas are necessary to get large water fluxes.

In this paper, we report both electrochemical experiments and results of computational fluid mechanics to improve spacer design. We then use these experiments and computations to develop a predictive model for spacer design. Because this is an important problem, we can build on earlier efforts by many other investigators. Many earlier experiments focus on bulk mixing in the thin channels. For example, Stroock et al. [4] used herringbone asymmetric-shaped spacers to improve mixing in micrometer-sized flow reactions. Hickey and Gooding [5] measured pervaporation fluxes for 15 different commercially available spacers, carefully considering how increases in mass transfer resulted in increases in pressure drop. Phattaranawik et al. [6] made similar studies for ultrafiltration, showing mass transfer increases of 60%. Xu et al. [7] made similar experiments for heat transfer, not with spacers but with longitudinal and lateral grooves cut in the walls of the heat exchangers. Schwinge et al. [8–10] studied mass transfer with zigzag-shaped spacers. Ahmad and Lau [11] found that spacers with cylindrical cross-section reduce concentration polarization better as compared to those with triangular and rectangular cross-sections. Li et al. [12] got their best results with a combination of non-woven spacers near the walls and a helical spacer in the center. Balster et al. [13] looked at a three-layered spacer, and like Li et al. [12] found enhanced performance as compared to single-layered net-type spacers. Da Costa and Fane [14], using diamond-shaped spacers for ultrafiltration, found the best results for spacers which cause fewer changes in flow direction, in apparent conflict with other results.

Computational fluid mechanics has produced a similar spectrum of results, especially for the heat transfer analogues of

* Corresponding author. Tel.: +1 612 625 1596; fax: +1 612 626 7246.
E-mail address: cussler@cems.umn.edu (E.L. Cussler).

0376-7388/$ – see front matter © 2008 Elsevier B.V. All rights reserved.
doi:10.1016/j.memsci.2008.05.060

concentration polarization. Many of these computations were by the same groups which performed the experiments summarized above. For example, Li et al. [15] made two-dimensional computations to optimize spacer design, including the best angular orientation. Sawyers et al. [16] showed how two-dimensional sinusoidal corrugations and three-dimensional "egg carton" corrugations can enhance heat transfer 25%. Kirtland et al. [17] concluded that two-dimensional simulations are inadequate to explain why three-dimensional herringbones enhance mass transfer at channel walls. Other numerical studies aiming at finding effects of spacers on mixing inside a channel and at the walls show common results. For example, Zhou et al. [18] developed a concentration polarization model for spirally wound reverse osmosis membrane modules which gives insight into the mixing effects of the spacers at the channel walls. Koutsou et al. [19] and Shakaib et al. [20] looked at the effects of different geometrical parameters of net-type spacer geometries on pressure drop, shear stresses and recirculation zones inside the channel. Kang and Kwon [21] verified the results of Stroock et al. [4] for staggered herringbones spacers by employing a colored particle with an algorithm to study concentration profiles in the bulk of the channel. Wang et al. [22] studied microchannels with patterned grooves numerically via three-dimensional CFD simulations and particle tracking techniques and concluded that the rotation effects produced by the grooves in the microchannels cause passive mixing. Yoon et al. [23] found similar results. Santos et al. [24] found that disruptions perpendicular to the flow were much more effective than disruptions parallel to the flow and buttressed their simulations with pressure drop measurements.

Each of these studies predicts how mass transfer might be enhanced in a particular situation. However, for us, none provides a simple, if approximate, rationale improving spacer design. We will seek such a rationale here, based on the experiments and simulations which are described next.

1. Experiments and simulations

The research described in this paper is based on electrochemical experiments and on computational fluid mechanics simulations. The electrochemical experiments were based on the familiar ferrocyanide reaction:

$$Fe(CN)_6^{-4} \rightleftharpoons Fe(CN)_6^{-3} + e \quad (1)$$

The computational fluid mechanics was based on FEMLAB. A synopsis of these efforts is given here; further details are available elsewhere [25].

1.1. Electrochemical experiments

Potassium hydroxide (Mallinckrodt) and carbon tetrachloride (EM Science) were reagent grade and used as received. Potassium hexacyanoferrate trihydrate (Fluka) and potassium ferricyanide (Aldrich) were 99.5% and 99.0% pure, respectively. Water was doubly distilled and sparged with nitrogen. Solutions were prepared by weight: a typical solution was 0.01 M K_4 $Fe(CN)_6$, 0.01 M K_3 $Fe(CN)_6$ and 0.5 M KOH.

The apparatus used for the experiments is shown schematically in Fig. 1. For rectangular channel experiments, it consists of a channel carved between two polycarbonate blocks and sealed with a rubber gasket. The channel is 10 cm long, 4 cm wide, and 1.5 mm high. The working and the counter electrodes, cut out of platinum sheet (Aldrich, 0.05 mm thick, 99.9+ percent), are 3 cm long and 1 cm wide. These are glued to the channel walls 1.5 cm away from the edges to reduce edge effects. A saturated calomel electrode was used as the reference electrode. The spacers, placed on one of the electrodes, are exemplified by those in Fig. 2. These were made by fused deposition modeling, a form of rapid prototyping. To make such a spacer, we first generated files defining the shape desired using CAD software (ProEngineer, Tristar, Phoenix, AZ). These files are fed to a computer linked to a rapid prototyping printer (Stratasys, Eden Prairie, MN, model Prodigy Plus). The printer extrudes a 1-mm ABS thread through a heated nozzle to make the desired shape. Typically, 10 spacers are made simultaneously in 3 h.

The experiments used the standard limiting current technique [26–28], with the working, counter, and reference electrodes connected to a potentiostat (Princeton Applied Research, Oak Ridge, TN, Model 363). The voltage was varied to determine limiting current plateaus (EG and G, Wellesley, MA, Parc Model 175 universal programmer). The flow of the aqueous solution, pumped with a syringe pump (Cole Palmer, Vernon-Hills, IL, 74900 series), was measured by recording the time to pump 50 ml. These times were reproducible to ±3%. To begin an experiment, we first prepared a fresh batch of electrolyte which was stored in photoresistant bottles. The electrodes were cleaned with carbon tetrachloride, the cell was assembled, and the experiment was begun. All experiments were made at 23 °C in reduced light to minimize photodegradation. Normally, the current was measured at five different flow rates for each spacer geometry. Repeated experiments showed that these currents were reproducible to within ±2%. Typical data for current as a function of voltage are shown in Fig. 3. At low voltage, the current is limited by the kinetics of the electrochemical reaction, which is not of interest here. At very high voltage, the current is a result of side reactions, especially of the hydrolysis of water. At intermediate voltages, the current is a plateau independent of voltage because it

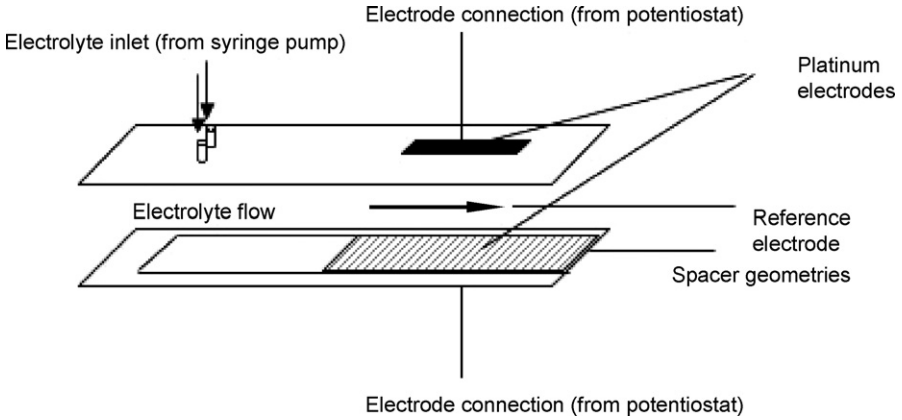

Fig. 1. The rectangular channel used in the electrochemical experiments. The plateau in measured current vs. potential is a measure of the mass transfer coefficient.

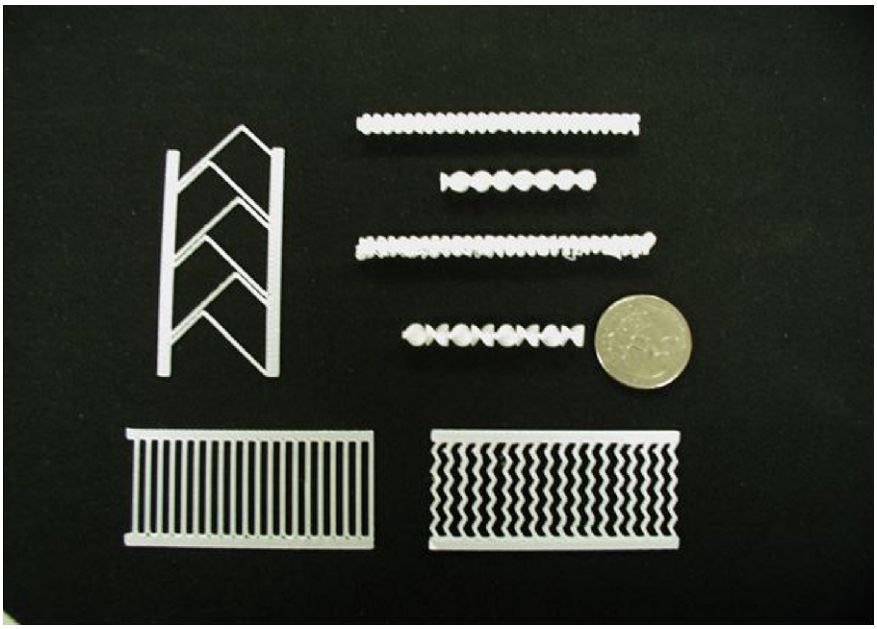

Fig. 2. Typical spacer designs. These were made by fused deposition modeling.

is limited by mass transfer. This is the region which is of interest here.

We can calculate the mass transfer coefficient k from the current I in this plateau from the equation:

$$k = \frac{I}{A\bar{c}_1 F} \tag{2}$$

where I is the limiting current in the plateau region, A is the area of the working electrode, $\bar{c}_1$ is the bulk ferricyanide concentration in solution, and F is Faraday's constant. Note that k is averaged over the entire area of the electrode. Note also that k will have the same value whether ferricyanide is being reduced or ferrocyanide is being oxidized, because the diffusion coefficients of these two species are almost the same. Finally, note that the data show that k rises as the flow is increased because concentration polarization is reduced. We will return to this point in Section 2.

1.2. Simulations

The simulations for different spacer geometries solve the mass balance

$$0 = -\boldsymbol{v} \cdot \nabla c_1 + D\nabla^2 c_1 \tag{3}$$

where $\boldsymbol{v}$ is the local solution velocity, c_1 is the local solute concentration, and D is the solute's diffusion coefficient. There is no term for diffusion-generated convection because the solutions are dilute. Eq. (3) is solved for flow in two-dimensions using FEMLAB. This computational multiphysics software utilizes the finite element method with adaptive meshing and automatic error control to solve coupled partial differential equations describing a particular physical model. The physical model, which can use equations in more than one physical domain, is suitable for simulations of fluid mechanics, mass transfer, electrodynamics, etc. It is linked to MATLAB which can be utilized for post-processing of results.

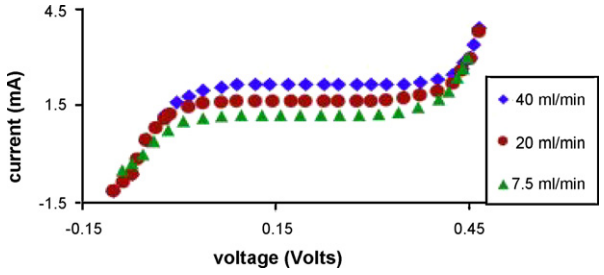

Fig. 3. Limiting current plateaus for different flow rates. The plateau on these figures is used in Eq. (2) to calculate the mass transfer coefficient k.

The calculations were different for different geometries. For empty rectangular channels, the concentration profile is obtained by solving the Navier–Stokes equations and the convection–diffusion equation inside the domain. First the velocity profile is calculated by solving the Stokes equations (i.e., the Navier–Stokes equations but for $Re = 0$) with no-slip boundary conditions at the walls and a pressure difference between the inlet and the outlet. This velocity profile is then used as an input to the convection–diffusion equation inside the rectangular channel. The boundary conditions include an infinitely fast reaction at the walls where $c_1 = 0$ and an inlet boundary condition of $c_1 = c_{10}$, which represents the species concentration entering the channel. The Peclet number in these calculations is high ($\sim$10,000), as in our experiments a high Peclet number implies that the mass transfer boundary layer is thin. In order to capture the sharp gradient in this thin mass transfer boundary layer, the meshing is refined at the walls by using the adaptive mesh technique, built into FEMLAB.

The calculations for two-dimensional, ladder-filled channels differed mainly in the boundary conditions. The ladder is attached to the bottom surface. The surface of these ladders is taken as impermeable to mass transfer, i.e., $(\partial c_1/\partial y) = 0$. The top wall and the space between the ladder rungs have infinitely fast reaction so concentration is zero there ($c_1 = 0$). The inlet again has constant concentration $c_1 = c_{10}$.

As in the case of empty rectangular channels, the Stokes flow equation with no-slip boundary conditions at the walls and specified pressure at the ends is solved first to get the velocity profile. This is then combined with the convection–diffusion equation to obtain the concentration profile inside the ladder-filled channel. Again, the adaptive meshing technique is used because the concentration gradients near the ladder surface and the walls are higher

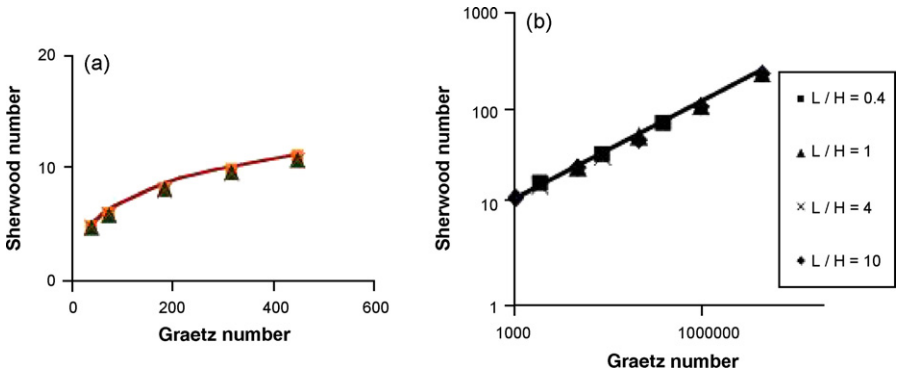

Fig. 4. Experiment vs. theory for an empty channel. The results in (a) are electrochemical; those in (b) are simulations.

than those in the bulk. Local mass transfer coefficients are found from Eq. (4).

$$k_x = \frac{D}{c_{1b}} \left. \frac{dc_1}{dy} \right| y = 0 \tag{4}$$

where c_{1b} is the cup mixing concentration in the channel. The average mass transfer coefficient is obtained as a function of position as in the case of an empty rectangular channel. However, unlike the empty channel where the mass transfer coefficient is same for both the top and bottom walls of the channel, the mass transfer coefficient is now calculated separately for each wall. This is done because the bottom wall is partly covered with ladder structures, and the top wall is not. The average mass transfer coefficient in each case is calculated from:

$$k = \frac{\int_{\text{free area}} k_x dx}{\int_{\text{free area}} dx} \tag{5}$$

where k_x is the local mass transfer coefficient evaluated at an axial location x. In all simulations, the mesh is refined until the concentration profile is independent of mesh size. The simulation is performed on a P4 3.4 GHz machine with a 2-GB RAM.

2. Results

Using the methods described above, we made four groups of experiments and simulations. First, we measured and calculated mass transfer coefficients in an empty rectangular channel, which allows comparison with a known analytical solution. Then we made experiments with three types of spacers: rectangular ridges placed perpendicular to the flow ("ladders"); similar asymmetric ridges placed at different angles to the flow ("herringbones"); and helically shaped spacers which tended to rotate the flow ("helices"). The results for all of these cases are summarized below; further details and pictures of the simulation results are given elsewhere [25].

2.1. Comparisons with analytical results

Mass transfer in a thin, empty channel has been very carefully studied, especially for short tubes. These studies are associated with Lévêque [29], who made the earliest calculations for a short cylindrical tube. The results for a rectangular slit whose width W is large relative to its height H are also well known [30]:

$$\left(\frac{kH}{D}\right) = 1.47 \left(\frac{H^2 v_o}{DL}\right)^{1/3} \tag{6}$$

where k is the average mass transfer coefficient at the channel walls, D is the diffusion coefficient in the fluids; v_o is the average fluid velocity; and L is the total channel length. The quantity in parentheses on the left-hand side of this equation is the Sherwood number; that on the right is the Graetz number. This result and its parallels for other cross-sections have been carefully verified, both for heat transfer and for mass transfer. It is a standard for testing the experiments and simulations.

The electrochemical experiments with an open rectangular channel are plotted in Fig. 4a. In this figure, the Sherwood number is shown on the ordinate, and the Graetz number is shown on the abscissa. The different symbols are the results of different experiments, and the solid line is a calculation from Eq. (6) made using the experimentally measured value of D equal to 0.73×10^{-9} m^2/s [31]. The close agreement between the electrochemical data and the equation is evidence that the experiments are working as expected.

The fluid mechanics simulations for similar open channels are shown in Fig. 4b. Again, the ordinate is the Sherwood number, a function of k; and the abscissa is the Graetz number, a measure of the flow. Now, the different symbols represent repeated simulations made at different ratios of slit length L to height H. As before, the solid line is the analytical prediction based on Eq. (6) and agrees closely with the simulations.

2.2. Ladder-type spacers: electrochemical experiments

With this basis in place, we now turn to results for different spacers. We first consider ladders, i.e., rectangular barriers made by fused deposition modeling and glued to the bottom electrode. These ladders are specified using the parameters defined in Fig. 5. In particular, the lengths that define these spacers are the entrance and exit lengths L_{ent} and L_{exit}, the spacing s between the ladder

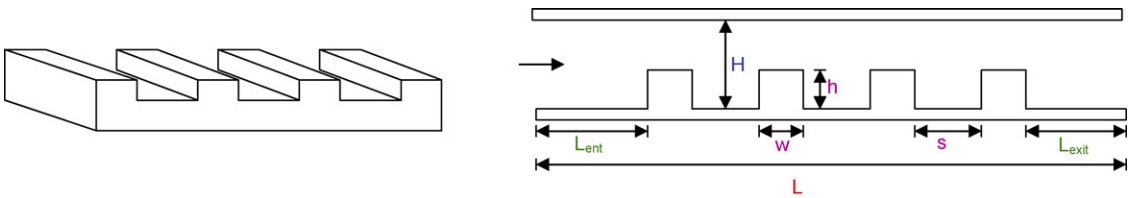

Fig. 5. Ladder type spacers. The spacer geometry is defined by the dimensions shown.

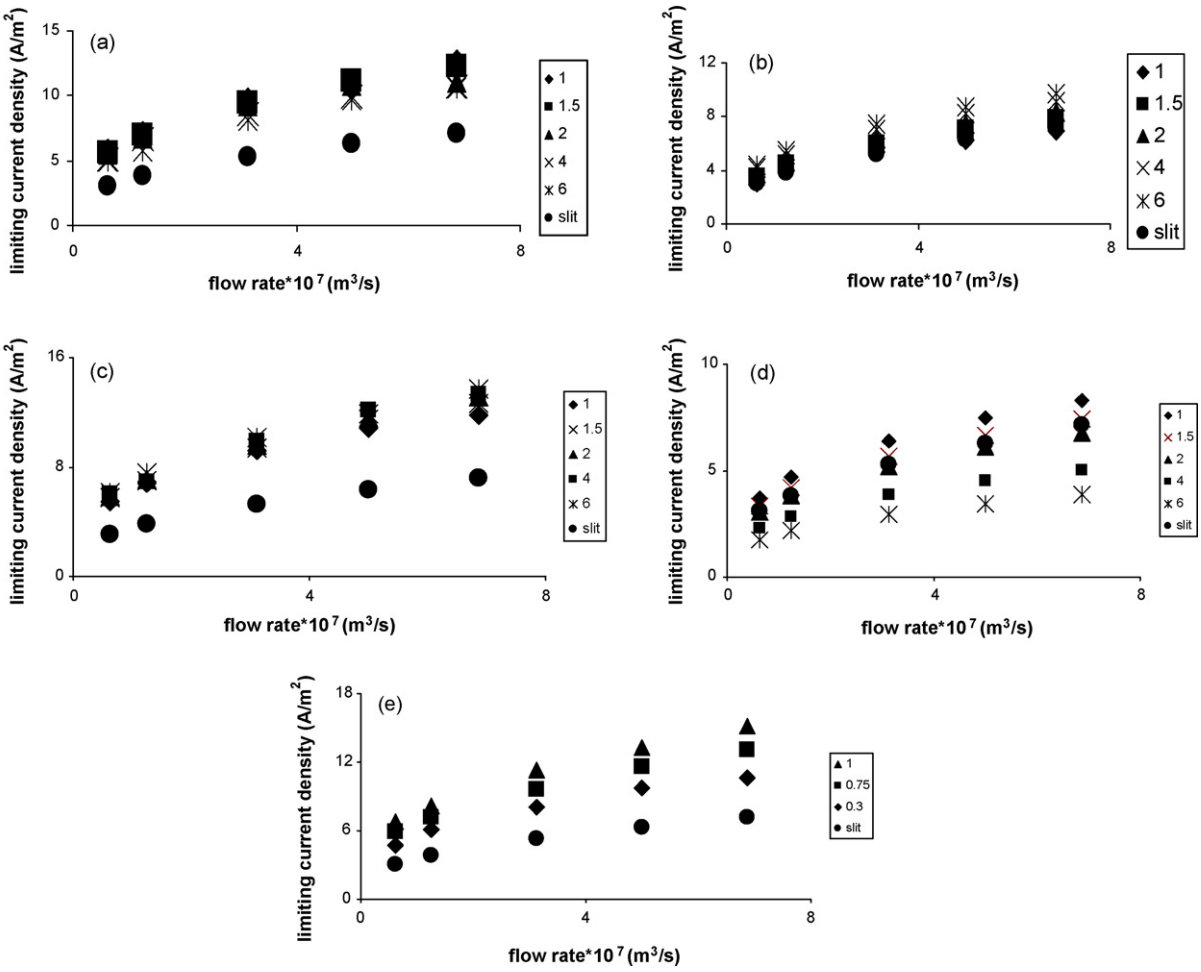

Fig. 6. Limiting current densities for different ladder spacers. (a) Top wall for ladders with different spacings (mm) fixed width (1 mm) and fixed height (0.75 mm); (b) top wall for ladders with different widths (mm), fixed height (0.75 mm) and fixed spacing (2 mm); (c) bottom wall with different spacings (mm), fixed height (0.75 mm) and fixed width (1 mm); (d) bottom wall with different spacings (mm), fixed height (0.75 mm) and fixed width (1 mm); and (e) top wall with different heights (mm), with fixed width (2 mm) and fixed spacing (2 mm).

rungs, the width w of these rungs, the height h of the ladders, and the total height H of the channel.

The limiting current density is plotted vs. flow rate for different ladder-type spacers in Fig. 6. Fig. 6(a, b, and e) shows that the limiting current density at the top wall increases with decreasing rung spacing because the increasing number of ladder rungs causes regions of high velocity directly above the rungs. These high velocity regions increase the mass transfer and hence increase the limiting current for the top electrode. Fig. 6(c) and (d), which shows the limiting current density for the bottom electrode, depict the opposite trend. With decreasing ladder spacing, the limiting current density at the bottom wall of the channel decreases because more rungs cover the electrode area, making less available for mass transfer. Still, while the data are consistent, they are hard to comprehend without the analysis developed in the discussion below.

2.3. Ladder-type spacers: fluid mechanical computations

Simulations for ladder-type spacers give results similar to the electrochemical experiments in Fig. 6. However, the simulations give not only the average mass transfer coefficient but also the local mass transfer coefficient. As in the electrochemical experiments, the simulations presume that the spacer is attached to one (bottom) electrode. The surface of the spacer is assumed to have zero permeability; thus the flux normal to the spacer surface is always zero. In contrast, because the reaction is fast, the concentration at the surface of the electrode of interest is zero. The simulation then calculates the concentration profiles for the ladder chosen. From these profiles, we find the mass transfer coefficient.

The simulations are exemplified by those shown in Fig. 7. The geometry is shown in the top part of this figure. The concentration is also qualitatively shown; darker areas indicate higher solute concentrations, and lighter areas show lower concentrations

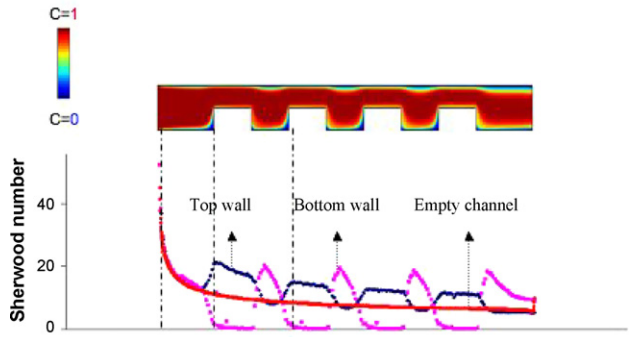

Fig. 7. The simulated concentration profile vs. the local Sherwood number for a ladder-filled channel. The smooth gray line represents the local Sherwood number in a slit without a spacer.

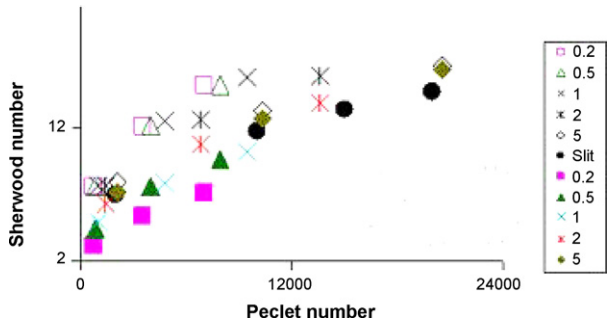

Fig. 8. Simulations of average Sherwood numbers for different ladders. Open symbols represent the top wall and the filled symbols represent the bottom wall.

where mass transfer occurs to the wall. Note how the concentration changes are sharper where the velocity is higher. Note also the recirculation zones of near zero flow where the ladder meets the bottom electrode. These recirculation zones are important. If the ladder rungs were spaced very close together, the zones could cover the entire electrode area, and the spacer would actually reduce the mass transfer.

The quantitative results are shown at the bottom of Fig. 7. The Sherwood number shown corresponds to the same position in the lower plot as in the upper one. It drops evenly for the empty channel, as shown by the gray points. When the channel is empty, the Sherwood number has the same value at the upper and lower boundaries. When a ladder-shaped spacer is present, the mass transfer coefficient is different on the top and bottom walls. At the top wall, it is higher above any of the rungs, as shown by the darker points. This increase, caused by the higher velocity, drops as the region nearest the wall is depleted. At the bottom wall, the mass transfer is highest at the upstream edge of any rung, as shown by the light gray points. It then drops quickly and is zero where the ladder's rung covers the electrode.

We made simulations for a similar range of ladder geometries to those studied electrochemically. Typical results, shown in Fig. 8, are for different ladder spacings. The open symbols are thus a mathematical parallel to those in Fig. 6(d); and the closed symbols are analogues to the experiments in Fig. 6(b). We will discuss these and other simulations in more detail in the next section of the paper. For now, we turn to different spacer shapes.

2.4. Staggered herringbone spacers

One of the most interesting alternatives to the simple ladder spacers are those called "staggered herringbones" or "staggered chevrons." These spacers are known to significantly enhance bulk mixing in small channels, and they may improve interfacial heat transfer as well [16]. Because they are asymmetric, they may generate a twisting, three-dimensional flow. The flow then depends not only on the height and spacing of the channel but also on the channel width perpendicular to the flow.

Electrochemical experiments conducted at different flow rates with the two different staggered herringbone spacers are shown in Fig. 9. The herringbone spacer shown on the left of Fig. 9 gives higher currents than that shown on the right, presumably because fluid elements close to the wall are more completely rotated from one vertex to the next. Thus as soon as one rotation is completed, the boundary layer is destroyed and redevelops as the next herringbone is encountered.

2.5. Helical spacers

Helical spacers manipulate the flow in the third dimension not by allowing the fluid to meander across the channel as herringbones do, but by forcing the fluid to twist along the channel. The result is a faster local velocity and a thinner mass transfer boundary layer. Such spacers, constructed using fused deposition modeling, were installed in a cylindrical channel 0.6 cm in diameter and 7 cm in length. The outer diameter of the spacers was the same as the inner diameter of the empty cylindrical channel. The central rod in the helix determines the inner wall of the channel. The electrodes are now two semi-circular strips measuring 0.95 cm across and 6.0 cm long, attached to the top and bottom of the cylindrical channel. The data for the electrochemical experiments conducted on different helical spacers are presented in Fig. 10. The best helical spacer gives mass transfer four times faster than that in an empty channel at the same flow rate, for the reasons discussed below.

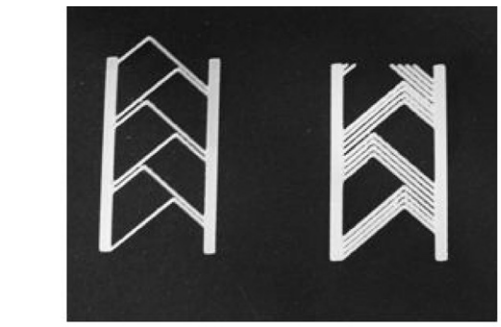

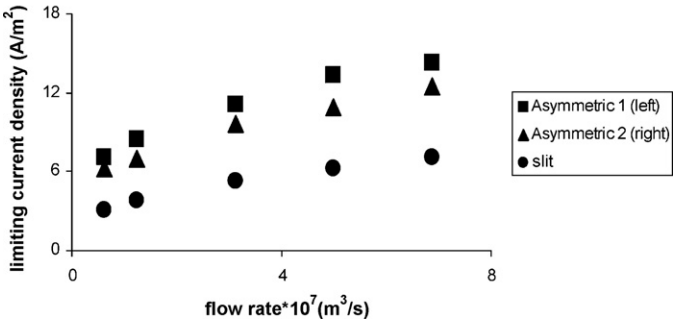

Fig. 9. Current in channel containing asymmetric spacers. The circles represent an empty channel, and the other symbols are for two asymmetric geometries.

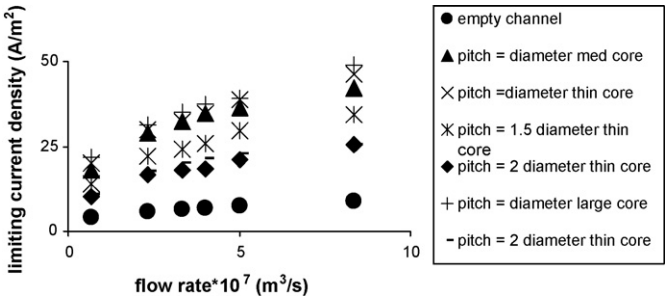

Fig. 10. Current for helical channels with varying pitch and core diameter. Note that large core gives the maximum mass transfer because of the smallest flow diameter at the same pitch.

3. Discussion

This work has two goals. First, we seek to show how specific spacer shapes can reduce concentration polarization and hence enhance ultrafiltration and reverse osmosis. Second, we hope to use results for specific spacers to develop a reliable guide for designing better spacers.

The results above show that we have succeeded in our first goal. We have made electrochemical measurements which give measurements of mass transfer accurate to within ±5% [25–28]. These mass transfer coefficients are an excellent measure of concentration polarization: large mass transfer coefficients mean small concentration polarization. We have shown that our measurements agree closely with well-established analytical solutions for mass transfer in a rectangular slit [29,30]. We have also measured the enhanced mass transfer caused by spacers of different geometries placed within the slit. These enhancements are least for spacers shaped like ladders, greater for spacers shaped like asymmetric herringbones, and greatest for spacers shaped like helices. We have also calculated the mass transfer coefficients in flows around ladder-shaped spacers using two-dimensional computational fluid mechanics. These results seem consistent with other earlier efforts [4–24].

However, the success of this first goal is incomplete for several reasons. The increased mass transfer is purchased at the cost of increased pressure drop [24]. More seriously, the mass transfer increases observed electrochemically may not translate directly to ultrafiltration and reverse osmosis because these are flow processes, not diffusion processes. Still, in the absence of phase separation, concentration polarization is a strong function of diffusion. The flow disruptions caused by ladder-shaped spacers do seem directly comparable, but those for helically shaped spacers may not be. The herringbone-shaped spacers are an intermediate case.

To see in more detail when the electrochemically experiments are limited, consider the specific reaction used here. In this reaction, ferrocyanate is oxidized at one electrode to ferricyanate. A helical flow then moves this ferricyanate-rich solution to the other electrode, where the ferricyanate is reduced to ferrocyanate. This is not what happens in ultrafiltration or reverse osmosis, where the electrodes are replaced by semi-permeable membranes. In the membrane case, a solute-rich region develops at one membrane, say at the bottom of the channel. If a helical flow moves this solute-rich region from the bottom membrane to the top one, it merely replaces one concentrated solution which retards separation with a second similar region which also retards separation. To be useful, helical spacers for ultrafiltration should transfer concentration from the wall to the bulk, not from one membrane to another. Similar arguments apply to the herringbone shaped spacers, though not as directly.

The more serious limitation of the research described so far is that we have not addressed our second goal: to provide an easy guide for improving spacer geometry. This guide should at least provide a rationale for better designs, and at most provide a means of evaluating them quantitatively. It should be simple to use, giving results with a handheld calculator.

To develop such a guide, we assume that any channel can be idealized as a series of short segments, each of which can be described with the Lévêque limit given in Eq. (6). This assumption implies that whenever the fluid encounters a new barrier, its concentration is instantly well mixed, and it behaves like a homogeneous solution entering a new tube. We make this assumption not because it seems an obvious approximation, but simply to start considering the effect of changes in cross-sectional area and of resulting changes in velocity.

To test this assumption, we consider in detail the results for the top electrode of a channel containing a ladder-shaped spacer with n rungs glued to the bottom electrode. The top electrode now consists of $(2n+1)$ channels connected end to end: one entrance channel; n channels where the bottom of the channel is a rung; $(n-1)$ channels between rungs where the channel bottom is the bottom electrode; and one exit channel. In each channel, the mass transfer coefficient can be found by rearranging Eq. (5). For the entrance and exit regions and for the $(n-1)$ regions between rungs, it is

$$k_i = 1.47\,\frac{D}{H}\left(\frac{HQ}{DL_i}\right)^{1/3} \tag{7}$$

where H is the channel height, Q is the volumetric flow per channel width, and L_i is the length of that particular channel. For the n regions above the rungs:

$$k_i = 1.47\,\frac{D}{H-h}\left(\frac{(H-h)Q}{Ds}\right)^{1/3} \tag{8}$$

where $(H-h)$ is the new open channel height, and s is the distance between rungs. On this basis, the overall mass transfer coefficient is just the sum of these contributions:

$$k_{\text{avg}} = \frac{\int k_i d\ell}{\int d\ell} = 1.47\,Q^{1/3}D^{2/3}\left[\frac{1}{L_{\text{ent}}^{1/3}H^{2/3}} + \frac{n}{r^{1/3}(H-h)^{2/3})} + \frac{n-1}{s^{1/3}H^{2/3}} + \frac{1}{L_{\text{exit}}^{1/3}H^{2/3}}\right] \tag{9}$$

Note $L(=L_{\text{ent}}+nr+(n-1)s+L_{\text{exit}})$ is the total length of the electrode. Note also that this implicitly neglects the effects of any spacers in the axial flow direction, consistent with other studies [24].

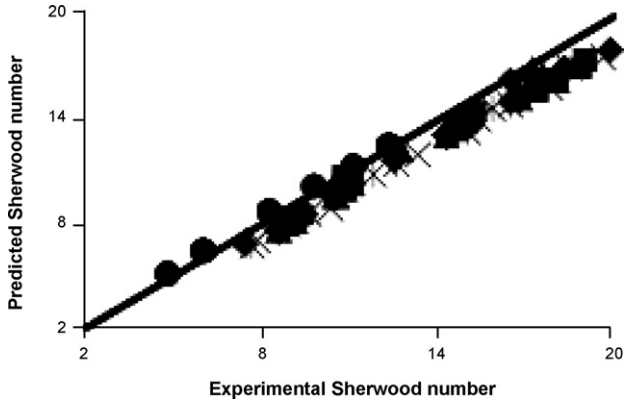

Fig. 11. Modified Lévêque limit for electrochemical mass transfer at the top wall. The data for the ladders are from Fig. 6(a), (b) and (e). The solid line is the prediction from Eq. (9).

The success of this idea is evaluated in Fig. 11, which plots the predicted mass transfer coefficient vs. that found experimentally. In other words, Fig. 11 uses Eq. (9) to replot all the data in Fig. 6(a), (b), and (e) on a single curve. No adjustable parameters are used in this replotting. The agreement between the predictions and the experiments is ±4%. For a bottom electrode partly obscured by ladder-shaped spacers, we get the same prediction as in Eq. (9) but without the term containing $[n/w^{1/3}(H-h)^{2/3}]$. The success of this prediction, accurate to ±4%, is given in Fig. 12, which replots the data in Fig. 6(c) and (d). The simulations of mass transfer with ladders are compared with predictions in Fig. 13. The agreement between prediction and computational fluid mechanics is again within 4%.

Lyster and Cohen [32] performed two-dimensional finite-element simulations of fluid flow and mass transport in rectangular and plate-and-frame channels in which one of the walls is permeable. For rectangular channels, they developed an empirical correlation between the average Sherwood number and the Reynolds and Schmidt numbers. Their correlation can be fit to the computational data using five adjustable parameters and reduces to

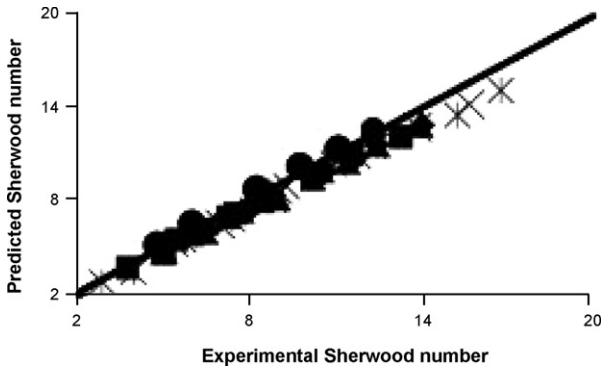

Fig. 12. Modified Lévêque limit for electrochemical mass transfer at the bottom wall. The data for the ladders are in Fig. 6(c) and (d). The solid line is the prediction from Eq. (9).

the classical Lévêque limit for the special case of zero permeate flux. For plate-and-frame channels, they noted the importance of recirculation regions in enhancing the likelihood of fouling. Although beyond the scope of the present work, we note that it may be possible to extend our approach to the case of permeable walls and thereby develop correlations that do not require adjustable parameters.

The predictions of mass transfer with herringbone or helical spacers are more speculative because these spacers generate more complex flows, and the Lévêque equation used here describes a two-dimensional flow. To make this jump, the characteristic length must be redefined. For the herringbones, the characteristic length is the repeat distance between chevrons L_{rot}, i.e., the distance which rotates the fluid completely. The height of the channel is that between the top electrode and the top of the herringbones ($H-h$). Thus the mass transfer coefficient is

$$k = \frac{1.47\,Q^{1/3}D^{2/3}}{L_{rot}^{1/3}}\left(\frac{1}{H-h}\right)^{2/3} \tag{10}$$

where Q is again the volumetric flow per channel width. The results for helical spacers are analogous. We consider only the case where the helix turns many times down the length of the channel. Again the flow is rotated in a distance L_{rot}

$$L_{rot} = w\sec\theta \tag{11}$$

where w is the electrode width and θ is the channel pitch. If the pitch is zero, the fluid does not move forward but simply rotates in place; if the pitch is 90°, the fluid does not rotate but passes straight through the channel. The height of the channel is the difference between the channel radius ($d_{channel}/2$) and the radius of the core of the helix ($d_{core}/2$). Thus the mass transfer coefficient

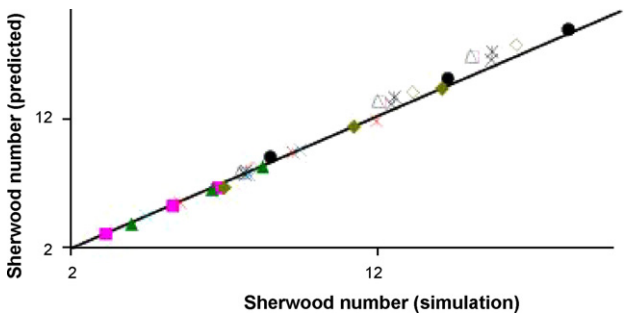

Fig. 13. Modified Lévêque limit for mass transfer with ladders. These data, from simulations, are taken from Fig. 8.

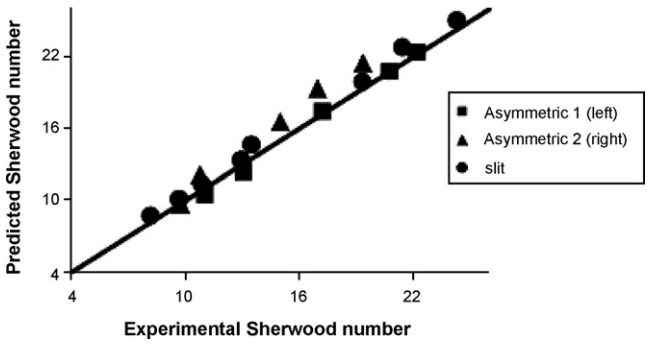

Fig. 14. Modified Lévêque limit for mass transfer with asymmetric spacers. These data, from Fig. 9, compare electrochemical results with predictions of Eq. (6).

from rearranging Eq. (5) is

$$k = \frac{1.47\,Q^{1/3}D^{2/3}}{(w\sec\theta)}\left[\frac{2}{d_{channel}-d_{core}}\right]^{2/3} \tag{12}$$

Eqs. (10) and (12) are the basis for predicting behavior of herringbone and helical spacers, respectively.

These predictions are tested in Figs. 14 and 15, respectively. The predictions for herringbones shown in Fig. 14 are within ±6% of the electrochemical values shown uncorrelated in Fig. 10. The predictions for helices, estimated from Eq. (12) and shown in Fig. 15, are within ±8% of the experimental values shown in Fig. 10. The differences between predicted and experimental values are larger for chevrons and helices than for ladder-shaped spacers, presumably a consequence of the three-dimensional, rotational flow caused by the non-ladder shapes.

The success of predictions based on these simple extensions of Lévêque's result fulfill the second goal of this paper. These extensions can predict the effect of new spacer designs without major effort. Eqs. (9), (10) and (12) or their analogues thus avoid large research efforts based either on electrochemical measurements or computational fluid mechanics. While such research efforts may sometimes be necessary, they can be made more productive using the ideas developed above.

The agreement of theory and experiment shown here is impressive, especially because it is obtained with simulations based on the assumption of zero Reynolds number. Although the Reynolds numbers in our experiments are finite, they are not large enough to cause significant deviations from the flow field that would be predicted by the Stokes equations (i.e., the zero-Reynolds number limit of the Navier–Stokes equations), which are the basis for our theoretical predictions. The fact that there is excellent agreement between theory and experiment provides clear evidence of this. Recircula-

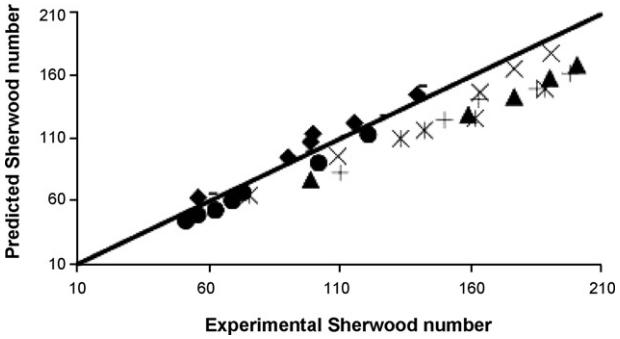

Fig. 15. Modified Lévêque limit for mass transfer with helical spacers. These data, from Fig. 10, correlate electrochemical results with predictions of Eq. (12).

tion regions certainly can exist in zero-Reynolds-number flows [33] and indeed these are observed in Fig. 7 [25]. From a practical viewpoint, the Stokes equations provide an appropriate model for flows that occur in geometries small enough so that inertial effects do not play a key role. Such geometries are becoming increasingly relevant to membrane separations and other transport processes as the drive toward miniaturization of chemical systems continues [34,35]. Although prior studies on membrane spacers considered flows with larger Reynolds numbers than those used here, none provides a simple model for predicting how spacer geometry influences mass transfer. We believe that our model is novel and useful and provides a fruitful starting point for developing similar models aimed at describing situations where inertial effects do play a key role.

At the same time, this conclusion raises two interesting questions for which we have no answers now. First, why do these extensions work so well? While we are not sure, we believe that the results imply that the most important aspect of mass transfer is a fresh surface. Thus our results can be considered a laminar parallel to arguments for the surface renewal theory for turbulent mass transfer (where the flow becomes unstable). Both these cases lead to formation of recirculation zones.

To illustrate this for cases with low Peclet numbers, consider a channel filled with ladder-type spacers. The flow close to the edge of the ladder has a component which gives rise to a recirculation zone. The size of this recirculation zone depends on the local flow profile at the ladder's edge, which in turn depends on the height to spacing ratio for the ladders. For Stokes flow, i.e., a Reynolds number equal to zero, when the spacing to height ratio is less than a critical number, which our simulations show to be about three, the recirculation zones at the edges of two adjacent ladder rungs combine to form bigger recirculation zones. These bigger recirculation zones are detrimental to mass transfer because they reduce the concentration gradients at the walls [36]. The local Peclet number in this recirculation zone is low, giving rise to a thicker boundary layer. In these cases, the modified Lévêque limit will over-predict the mass transfer coefficient at the channel walls. However, in this paper the Peclet numbers for channels are high (>100), which is the basic assumption of the Lévêque limit for empty channels. For high Peclet numbers and for ladder spacing to height ratio greater than 3, the recirculation zones are small and cover a small fraction of the channel walls, which justifies the neglecting them while calculating the mass transfer coefficient. The modified Lévêque limit in this study, established for Stokes flow, will also under-predict the mass transfer at the walls of a spacer-filled channel for higher Reynolds numbers where flow instability occurs [37–40]. These instabilities again lead to recirculation zones in the fluid bulk, which have been shown to enhance the transport at the channel walls [37–40]. They are not in range of Peclet numbers covered by the experiments and simulations in this paper.

Finally, in a helical flow there are no flow obstructions at the channel walls so any recirculation zones that blind the channel walls are absent. Still, at high Reynolds numbers, secondary flow profiles in the channel bulk can cause mass transfer enhancement at the walls by accelerating the sweeping flow at the walls. For higher Reynolds number (>200), when the secondary flow profiles are significant [37], the modified Lévêque limit will under-predict the mass transfer coefficient at the channel walls. Still, for the high Peclet and low Reynolds numbers considered here, the Lévêque approximation works.

Our second question is still more speculative: are there any spacer designs which might work better still? Again, while we do not know, we are intrigued by ideas of non-rigid, elastic spacers. Under some conditions, these spacers can move chaotically, randomly disrupting the flows near the wall. Such chaotic motion may reduce concentration polarization in that region. We look forward to learning about this possibility.

Acknowledgments

Nathan Craig helped make the electrochemical measurements. The work was partially supported by the Petroleum Research Fund of the American Chemical Society. Other support came from the United States Air Force Office of Scientific Research.

References

[1] R.W. Baker, Membrane Technology and Applications, 2nd ed., Wiley, New York, 2004.
[2] W. Ho, K. Sirkar, Membrane Handbook, Springer, Berlin, 1992.
[3] A.W. Nienow, M.F. Edwards, N. Harnby, Mixing in the Process Industries, 2nd ed., Butterworths–Heineman, London, 1997.
[4] A.D. Stroock, S.K.W. Dertinger, A. Adjari, I. Mezic, H.A. Stone, G.M. Whitesides, Science 295 (2002) 647–651.
[5] P.J. Hickey, C.H. Gooding, Journal of Membrane Science 92 (1994) 59–74.
[6] J. Phattaranawik, R. Jiraratananon, Fane A.G., Journal of Membrane Science 217 (2003) 193–206.
[7] J.L. Xu, Y.H. Gan, D.C. Zhang, X.H. Li, International Journal of Heat and Mass Transfer 48 (2005) 1662–1674.
[8] J. Schwinge, D.E. Wiley, A.G. Fane, R. Guenther, Journal of Membrane Science 172 (2000) 19–31.
[9] J. Schwinge, D.E. Wiley, D.F. Fletcher, Industrial and Engineering Chemistry Research 41 (2002) 2977–2987.
[10] J. Schwinge, D.E. Wiley, D.F. Fletcher, Industrial and Engineering Chemistry Research 41 (2002) 4879–4888.
[11] A.L. Ahmad, K.K. Lau, Journal of Membrane Science 286 (2006) 77–92.
[12] F. Li, W. Meindersma, A.B. de Haan, T. Reith, Journal of Membrane Science 253 (2005) 1–12.
[13] J. Balster, I. Punt, D.F. Stamatialis, M. Wessling, Journal of Membrane Science 282 (2006) 351–361.
[14] A.R. Da Costa, A.G. Fane, Industrial and Engineering Chemistry Research 33 (1994) 1845–1851.
[15] F. Li, W. Meindersma, A.B. de Haan, T. Reith, Journal of Membrane Science 208 (2002) 289–302.
[16] D.R. Sawyers, M. Sen, H.-C. Chang, International Journal of Heat and Mass Transfer 41 (1998) 3559–3573.
[17] J.D. Kirtland, G.J. McGraw, A.D. Stroock, Physics of Fluids 18 (2006) 73601–73613.
[18] W. Zhou, L. Song, T.K. Guan, Journal of Membrane Science 271 (2007) 38–46.
[19] C.P. Koustsou, S.G. Yiantsios, A.J. Karabelas, Journal of Membrane Science 291 (2007) 53–69.
[20] M. Shakaib, S.M.F. Hasani, M. Mahmood, Journal of Membrane Science 297 (2007) 74–89.
[21] T.G. Kang, T.H. Kwon, Journal of Micromechanics and Microengineering 14 (2004) 891–899.
[22] H. Wang, P. Iovenitti, E. Harvey, S. Masood, Journal of Micromechanics and Microengineering 13 (2003) 801–808.
[23] S.K. Yoon, G.W. Fichtl, P.J.A. Kenis, Lab on a Chip 6 (2006) 1516–1524.
[24] J.L.C. Santos, V. Geraldes, S. Velizarov, J.G. Crespo, Investigation of flow patterns and mass transfer in membrane module channels filled with flow aligned spacers using computational fluid mechanics, Journal of Membrane Science 305 (2007) 103–117.
[25] A. Shrivastava, Faster Mass Transfer in Small Channels, PhD thesis, University of Minnesota, Twin Cities, 2007.
[26] T. Mizushina, Advances in Heat Transfer 7 (1971) 87–161.
[27] J.R. Selman, C.W. Tobias, Advances in Chemical Engineering 10 (1978) 211–308.
[28] F. Li, W. Meindersma, A.B. de Haan, T. Reith, Journal of Membrane Science 232 (2004) 19–30.
[29] M.A. Lévêque, Annales des Mines 13 (1928) 281, 201, 305.
[30] F. Kreith, M.S. Bohn, Principles of Heat Transfer, 6th ed., Harper and Row, New York, 2000.
[31] E.L. Cussler, Diffusion, 2nd ed., Cambridge University Press, Cambridge, 1997.
[32] E. Lyster, Y. Cohen, Journal of Membrane Science 303 (2007) 140–153.
[33] L.G. Leal, Advanced Transport Phenomena, Cambridge University Press, New York, 2007.
[34] T.M. Squires, S.R. Quake, Microfluidics: fluid physics at the nanoliter scale, Reviews of Modern Physics 77 (2005) 977–1026.
[35] H.A. Stone, A.D. Stroock, A. Ajdar, Engineering flows in small devices: microfluidics toward lab-on-a-chip, Annual Reviews of Fluid Mechanics 36 (2004) 381–411.
[36] L. Song, Ma Shengwei, Numerical studies of the impact of spacer geometry on concentration polarization in spiral wound membrane modules, Industrial Engineering and Chemical Research 44 (2005) 7638–7645.

[37] V. Geraldes, V. Semiao, M.N. Pinho, Flow management in nanofiltration spiral wound modules with ladder-type spacers, Journal of Membrane Science 203 (2002) 87–1002.
[38] C.P. Koutsou, S.G. Yiantsios, A.J. Karabelas, Numerical simulation of the flow in a plane-channel containing a periodic array of cylindrical turbulence promoters, Journal of Membrane Science 231 (2004) 81–90.
[39] C.P. Koutsou, S.G. Yiantsios, A.J. Karabelas, Direct numerical simulation of flow in spacer-filled channels: effect of spacer geometrical characteristics, Journal of Membrane Science 291 (2007) 53–69.
[40] D.R. Sawyers, M. Sen, H.C. Chang, Heat transfer enhancement in three-dimensional corrugated channel flow, International Journal of Heat and Mass Transfer 41 (1998) 3559–3573.